INTERNATIONAL JOURNAL FOR NUMERICAL METHODS IN FLUIDS, VOL. 11, 39–56 (1990)

THE CALCULATION OF INCOMPRESSIBLE SEPARATED TURBULENT BOUNDARY LAYERS

A. KOGAN AND S. MIGEMI

CFD Group, Israel Aircraft Industries, Ben Gurion Airport, Israel

SUMMARY

The algebraic turbulent model of Baldwin and Lomax was incorporated into the incompressible full Navier–Stokes code FIDAP. This model was extensively tested in the past in finite difference codes. We believe that the incorporation of the model also into the finite element code has resulted in a practical method to compute a variety of separated turbulent 2D flows. Firstly, we use the model to compute the attached flow about an aerofoil. Next, the application of the model to separated flows is presented by computing the flows at high angles of attack up to maximum lift. It is shown that the model is capable of predicting separation, steady stall and $C_{L\max}$. As a difficult test of the model we compute the laminar separation bubble development directly using the full Navier–Stokes finite element code. As far as we know, this approach has not yet been reported. The importance of using an appropriate upwinding is discussed. When possible, comparison of computed results with experiments is presented and the agreement is good.

KEY WORDS Aerodynamics Turbulence Separation $C_{L\max}$ Laminar Bubble

INTRODUCTION

In recent years, with the rapid increase of computing power, there has been an increasing demand in the aeronautical industry to use CFD codes to assist the engineer in evaluating the aerodynamic performance parameters such as lift and drag of various aerodynamic designs.

The main interest is in exterior flows with high Reynolds number, which are mainly turbulent. In this paper we treat the viscous flow about a two-dimensional aerofoil. We restrict our attention to steady incompressible flows. The viscous laminar flow about an aerofoil is governed by the steady Navier–Stokes and continuity equations

$$u_k \frac{\partial u_i}{\partial x_k} + \frac{1}{\rho}\frac{\partial p}{\partial x_i} = \frac{\partial}{\partial x_k}\left[\nu\left(\frac{\partial u_i}{\partial x_k} + \frac{\partial u_k}{\partial x_i}\right)\right], \tag{1}$$

$$\frac{\partial u_k}{\partial x_k} = 0. \tag{2}$$

For high-Reynolds-number flows the laminar boundary layer is absolutely unstable and undergoes transition to turbulence. Equations (1) and (2) are not directly soluble for turbulent flows and as usual we use the time-averaged form of these equations

$$\bar{u}_k \frac{\partial \bar{u}_i}{\partial x_k} + \frac{1}{\rho}\frac{\partial \bar{p}}{\partial x_i} = \frac{\partial}{\partial x_k}\left[\nu\left(\frac{\partial \bar{u}_i}{\partial x_k} + \frac{\partial \bar{u}_k}{\partial x_i}\right) - \overline{u_i' u_k'}\right], \tag{3}$$

$$\frac{\partial \bar{u}_k}{\partial x_k} = 0. \tag{4}$$

0271–2091/90/090039–18$09.00

Received 26 July 1989
Revised 25 September 1989

The Reynolds turbulent stress tensor

$$R_{ik} = -\overline{u_i' u_k'} \tag{5}$$

describes the influence of the fluctuating motion on the average motion. To close system (3) through (5), we must express R_{ik} in terms of known mean flow quantities. This task is known as turbulence modelling.

There are basically two approaches to turbulence modelling. The first approach uses algebraic relations to express R_{ik} with the help of u_k. The second approach uses additional transport equations derived from equations (1) and (2) for additional turbulent quantities to express the Reynolds stresses R_{ik}.[1-3]

Much experience has been gained over the years in the applicability of turbulence models to specific flows.[2] It is generally agreed that algebraic models do not take history and transport effects into account, in contrast to the case of turbulent transport equations. The most popular of the transport equation models is the two-equation k–ε model. However, the use of the k–ε equations in addition to (3) and (4) requires that boundary conditions be given for k and ε at the wall. At the wall k is zero since all velocities vanish there. In this case the solutions for k and ε would be zero everywhere. Therefore in principle the k–ε equations are not applicable at the wall region. It is necessary to supply boundary conditions for k and ε at some distance away from the wall.[2] Usually it is done at a normal distance y from the solid wall where the log law for the velocity applies. For separated exterior aerodynamic flows where the separation point is not known in advance, there is no certain velocity law of the wall and therefore the k–ε model in principle cannot be applied. The k–ε model has been successfully applied to confined flows, attached flows and recirculating flows because it is possible in these cases to supply reasonable boundary conditions for k and ε. For these reasons the modelling used for aerodynamic applications is mostly algebraic.

Of the various algebraic models, the most widely used are those of Cebeci and Smith[4] and Baldwin and Lomax.[5] The Cebeci–Smith model explicitly requires the use of boundary layer concepts such as δ^* and u_e and is therefore well suited for attached flows. The Cebeci–Smith model is not directly applicable to separating boundary layers. On the other hand, the Baldwin–Lomax is suitable for both attached and separated boundary layers because it does not require the definition of boundary layer quantities. The Baldwin–Lomax model has also been applied to compressible turbulent boundary layers.[6,7] It is known that when using the Baldwin–Lomax equilibrium model there is a discrepancy between computation and experiment in the case of separated flows, mainly because of the premature prediction of the separation point. The discrepancy has been demonstrated mainly for compressible flows with shock/boundary layer interaction.[8] For incompressible flows, where separation is due to the adverse pressure gradient, the discrepancy seems to be smaller, as demonstrated by our results and the results obtained using finite difference codes with the Baldwin–Lomax model.[6,9]

Once the turbulence model of Baldwin and Lomax was selected, a user routine was written and incorporated into the incompressible Navier–Stokes finite element code FIDAP. We have applied FIDAP plus the incorporated model to different types of incompressible 2D boundary layers developing on an aerofoil flying at low Re (1×10^6) to high Re (9×10^6). Firstly, the model was used to compute the attached viscous flow developing at low angles of attack about NACA 4415. Next, the model was used to compute the viscous flow at high angles of attack about aerofoils NACA 0012 and NACA 4415. The boundary layer in these cases is separated over large rear parts of the aerofoils' upper surface. The model could correctly predict $C_{L\max}$ for these aerofoils.

For certain aerofoils the transition from laminar to turbulent boundary layer is through a laminar separation bubble (LSB). The computation of LSB flows has for a long time been a

challenge to CFD codes. As far as we know, all others simulate LSB flows by using viscous/non-viscous interaction analysis.[13, 14] We use the full Navier–Stokes equations with the turbulence model to compute LSB flows directly. Following the physics of LSBs, we have developed a procedure to compute LSB flows over laminar aerofoils. The robustness of the procedure is also demonstrated by computing the LSB flow over an aerofoil at high angles of attack and by comparing the C_p with experimental results.

Although the most important factor in successfully predicting separated flow is a successful model, the upwinding used in the numerical method may have a great effect on the results of the flow simulation. Therefore the choice of a suitable upwinding is quite important. The upwinding used in FIDAP is a streamline upwinding developed by Brooks and Hughes.[10] Certain features of this upwinding are discussed below.

THE TURBULENCE MODEL

As noted, The Baldwin–Lomax algebraic model[5] is used in all the computations described below. Originally, this model was developed for the calculation of compressible boundary layers using finite difference codes. This model was introduced in 1978 but only in the last few years has it been widely used in Navier–Stokes codes to calculate turbulent separated flows.[6, 7] This model has escaped the attention of researchers in incompressible flows and especially of those using finite elements codes such as FIDAP to solve the Navier–Stokes equations. An important review of turbulent models[2] for incompressible flows did not include this model. However, this model has proven successful in computing practical aerodynamic flows such as turbulent separated flows. We describe the model for 2D flows although in principle it can be applied to 3D flows. For convenience we drop the bar denoting mean values and all variables appearing below are mean flow quantities. To express the Reynolds stresses R_{ik} by means of mean velocities, one uses the Boussinesq eddy viscosity concept:

$$-\overline{u_i' u_k'} = \nu_t(x_1, x_2)\left(\frac{\partial u_i}{\partial x_k} + \frac{\partial u_k}{\partial x_i}\right), \quad i = 1, 2. \tag{6}$$

Unlike in (3), the turbulent viscosity coefficient $\nu_t(x_1, x_2)$ depends on the co-ordinates and is defined semi-empirically by the model. Any algebraic model must take into account the structure of the turbulent boundary layer, which consists of inner and outer layers. The inner layer is adjacent to the wall, where the length and velocity scales are defined by the shear viscosity at the wall. The scales in the outer layer depend on the local main flow and to some extent on the flow history. The eddy viscosity is written

$$\nu_t = \begin{cases} \nu_{t_o}, & y > y^x, \\ \nu_{t_i}, & y < y^x, \end{cases} \tag{7}$$

where ν_{t_i} and ν_{t_o} are the turbulent viscosities of the inner and outer layers respectively. The value y^x is the smallest value of y at which the inner and outer formulae are equal.

For the inner layer the Prandtl–Van Driest formulation is used:

$$\nu_t \sim L^2 \left|\frac{\partial u}{\partial y} - \frac{\partial v}{\partial x}\right|, \qquad L \sim k y\left[1 - \exp\left(\frac{-y^+}{A^+}\right)\right], \tag{8}$$

where

$$y^+ = \frac{y}{y_\tau}, \qquad y_\tau = \nu\left(\nu\left|\frac{\partial u}{\partial y} - \frac{\partial v}{\partial x}\right|_{y=0}\right)^{-1/2}.$$

For the outer layer

$$\nu_{t_o} = \alpha C_1 F_{\text{Kleb}} y_{\max} F_{\max} \text{Min}\left[1, \frac{1}{4}\left(\frac{U_{\max} - U_{\min}}{F_{\max}}\right)^2\right], \tag{9}$$

where $\alpha = 0{\cdot}0168$, $C_1 = 1{\cdot}6$, F_{Kleb} is the Klebanof intermittency function,

$$F_{\text{Kleb}} = 1/[1 + 5{\cdot}5(0{\cdot}3y/y_{\max})^6],$$

$F_{\max}$ is the maximum value of the vorticity function,

$$F(y) = \left|\frac{\partial u}{\partial y} - \frac{\partial v}{\partial x}\right| y\left[1 - \exp\left(\frac{-y^+}{A^+}\right)\right], \tag{10}$$

$y_{\max}$ is the y-location of $F_{\max}$, and $U_{\max}$ and $U_{\min}$ are the maximum and minimum velocities in a profile normal to the surface.

In the above formulation the co-ordinates x and y are tangential and orthogonal to the profile respectively. Therefore we require that the mesh lines within the turbulent layer should be orthogonal to the profile. This has been done using FIDAP grid generation.

THE NUMERICAL METHOD

As the basic Navier–Stokes code we have applied FIDAP with the algebraic model incorporated into it. FIDAP is a finite element code for the incompressible Navier–Stokes equations. For turbulent steady flows the equations of conservation of momentum are written in the stress divergence form

$$\rho u_k \frac{\partial u_i}{\partial x_k} = \frac{\partial \tau_{ik}}{\partial x_k}, \qquad \tau_{ik} = -p\delta_{ik} + \tilde{\mu}\left(\frac{\partial u_i}{\partial x_k} + \frac{\partial u_k}{\partial x_i}\right). \tag{11}$$

For simplicity, instead of the continuity equation (4) we use the pressure penalization[11,12]

$$p = \frac{1}{\beta}\frac{\partial u_k}{\partial x_k}, \tag{12}$$

with penalty parameter $\beta = 10^{-9}$–10^{-8}. Equations (11) are solved by the Galerkin method in the finite element approximation. The resulting system of non-linear equations is solved by the method of successive approximations.

The computational grid

An important step before the solution of the Navier–Stokes equations is the generation of a suitable grid. For high-Reynolds-number turbulent flows the boundary layer is very thin and because of the no-slip condition the velocity gradient has a very steep component normal to the surface. Therefore we must have high grid resolution normal to surface. Usually the height δy of the first cell above the aerofoil is $0{\cdot}00006c$, where c is the aerofoil chord. The second requirement is that the grid lines should be orthogonal to the surface within the entire boundary layer. This is because the Baldwin–Lomax model is defined for velocity profiles normal to the aerofoil's surface. An example is given in Figure 1.

On the average, 19 grid points are used inside the boundary layer out of a total of 30 points in the y-direction. An important point is the value of δx, the cell size in the direction tangential to the surface, and consequently of the grid aspect ratio $\delta y/\delta x$. With 200 points around the aerofoil the

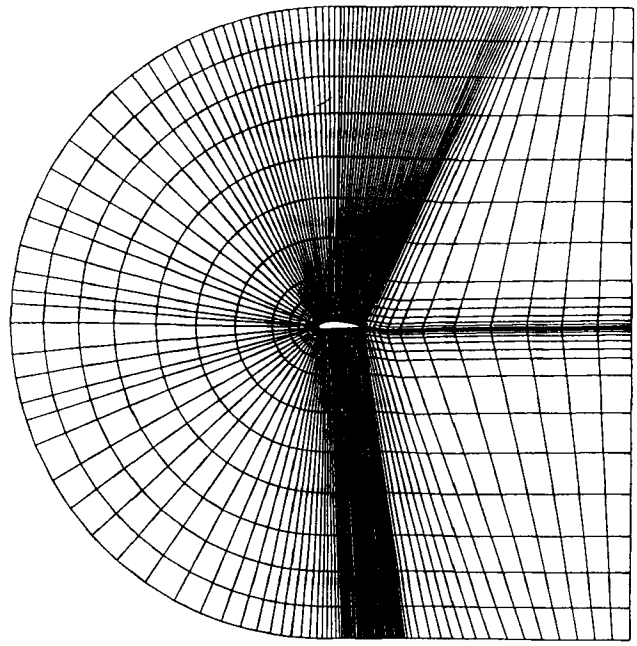

(a)

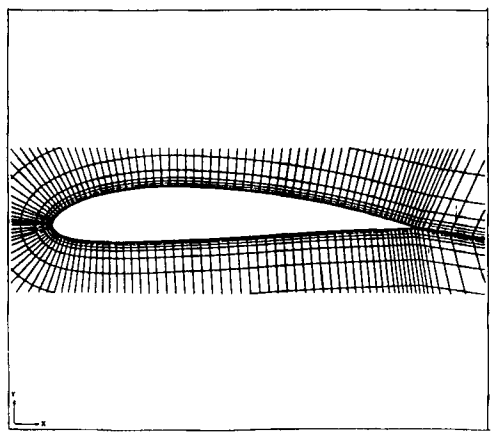

(b)

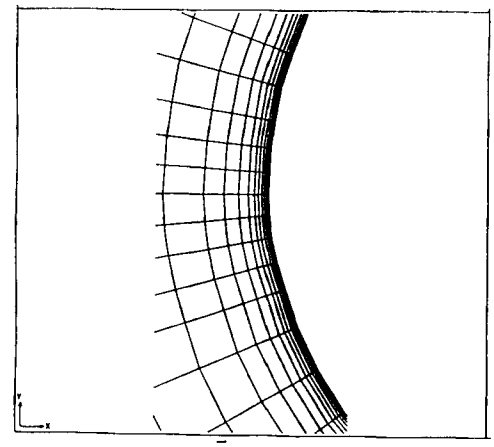

(c)

Figure 1. Grid generation for turbulent flow calculations: (a) overall grid about NACA 4415; (b) grid points near the aerofoil; (c) grid points at the leading edge

grid aspect ratio is about 200. A total of about 7100 grid points are used in the 2D problem. The grid points are used as nodes of quadrilateral elements to form isoparametric finite elements (Figure 1).

Boundary and initial conditions

A sketch of the computational domain is given in Figure 2. The aerofoil is placed inside the computational domain. At infinity the computational domain is bounded by lines EF and DG about 6 aerofoil chords away from the aerofoil. The top and bottom boundaries are 6 aerofoil chords away from the aerofoil. For incompressible flow the pressure is defined up to an additive constant. Since the velocity is a constant vector at infinity, it follows from (12) that the constant is defined in such a way that

$$p(\infty)=0. \tag{13}$$

On the aerofoil ABC we have the no-slip condition

$$u_i|_{\mathrm{ABC}}=0. \tag{14}$$

On the part DEFG of the far field boundary we prescribe the free velocity condition

$$u_1(\infty)=u_\infty \cos\alpha, \qquad u_2(\infty)=u_\infty \sin\alpha, \tag{15}$$

where u_∞ is the velocity at infinity and α is the angle of attack. On the part DG, normal zero-stress conditions are applied:

$$\tau_{ik}n_k=\left[-pn_i+\tilde{\mu}\left(\frac{\partial u_i}{\partial x_k}+\frac{\partial u_k}{\partial x_i}\right)n_k\right]\Bigg|_\infty=0, \tag{16}$$

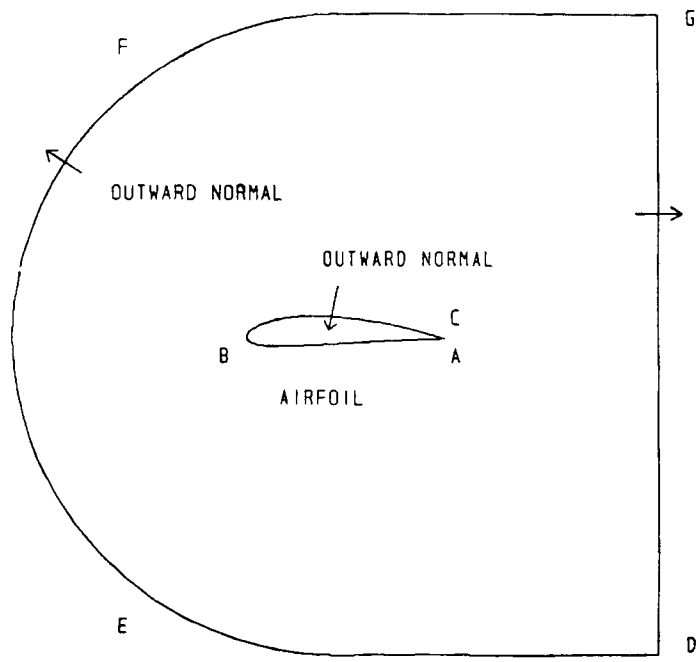

Figure 2. Boundary and initial conditions for Navier–Stokes equations

where n_k is the outward-pointing normal unit vector and p is defined by the penalty relation (12) everywhere. For the steady state solution we specify as initial conditions the free velocity at infinity.

Upwinding

All aerofoil codes for solving the Navier–Stokes equations use some form of artificial viscosity (or upwinding) for numerical stability. High-Reynolds-number flows are flows with small molecular viscosity. The artificial viscosity added for numerical stability may wholly misrepresent the structures and scales of turbulent boundary layers to give a wrong flow picture. In FIDAP the artificial viscosity has the form of streamline upwinding.[10] This means that the longitudinal artificial stress

$$v_{\text{art}} \frac{\partial u}{\partial x}, \tag{17}$$

where v_{art} is proportional to the mesh size δx, is added to the molecular stress

$$v \frac{\partial u}{\partial x}. \tag{18}$$

On the other hand, there is no contribution of artificial viscosity to the real shear normal stress

$$v \frac{\partial u}{\partial y} \tag{19}$$

acting across the boundary layer. Consequently the artificial viscosity does not effect the turbulent viscosity coefficient in the Baldwin–Lomax model.[5]

The longitudinal derivative of the artificial stress, $(\partial/\partial x)(v_{\text{art}}\, \partial u/\partial x)$, adds an artificial force to the pressure gradient and to some extent this may have an influence on the separation point on the aerofoil. To reduce this effect it is necessary to refine the mesh in the longitudinal direction.

RESULTS

Although in principle the model can be applied to 3D turbulent flows, the 2D version as described above was incorporated into FIDAP and applied to a variety of 2D high-Reynolds-number shear turbulent flows: attached and separated flows, C_{Lmax} prediction and laminar separation bubble flows. We give below the results of such flow simulations.

Attached turbulent flows

The attached turbulent flow at $Re = 9 \times 10^6$ about the NACA 4415 aerofoil for angles of attack of 0° and 4° was calculated using the well-known Korn–Garabedian 2D code and FIDAP. The Korn code solves the flow by viscid/inviscid interaction analysis. The turbulent boundary layer is computed by the Nash–Macdonald integral method. Streamlines of the flows as calculated by FIDAP are given in Figure 3. It is seen that in both cases the flow is attached to the aerofoil. The comparison of the C_p distribution as computed by the two programs is given in Figure 4. It is seen that the agreement is good.

Flow separation and C_{Lmax} prediction

As the angle of attack is increased, the adverse pressure gradients increase and eventually the flow separates. For aerofoils such as NACA 0012 and NACA 4415 the separation starts at the

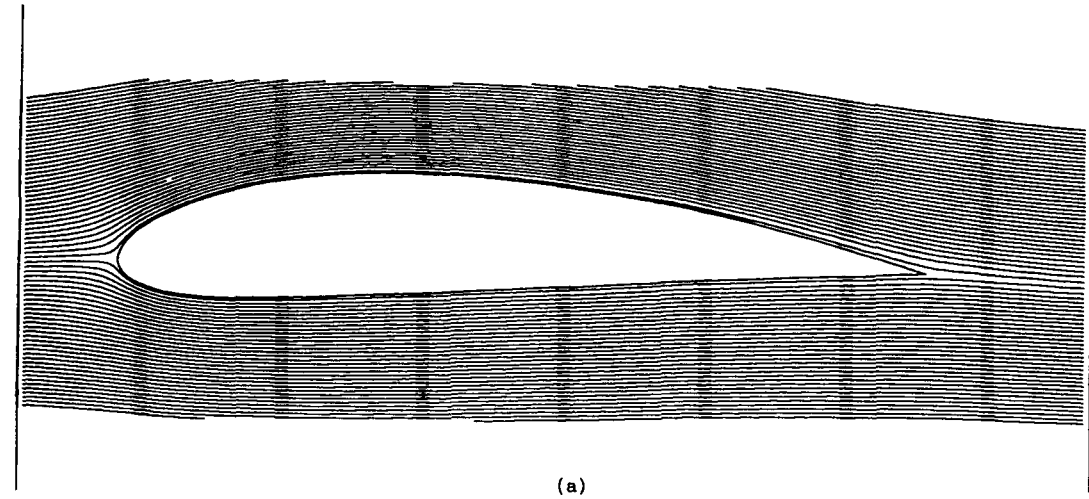

(a)

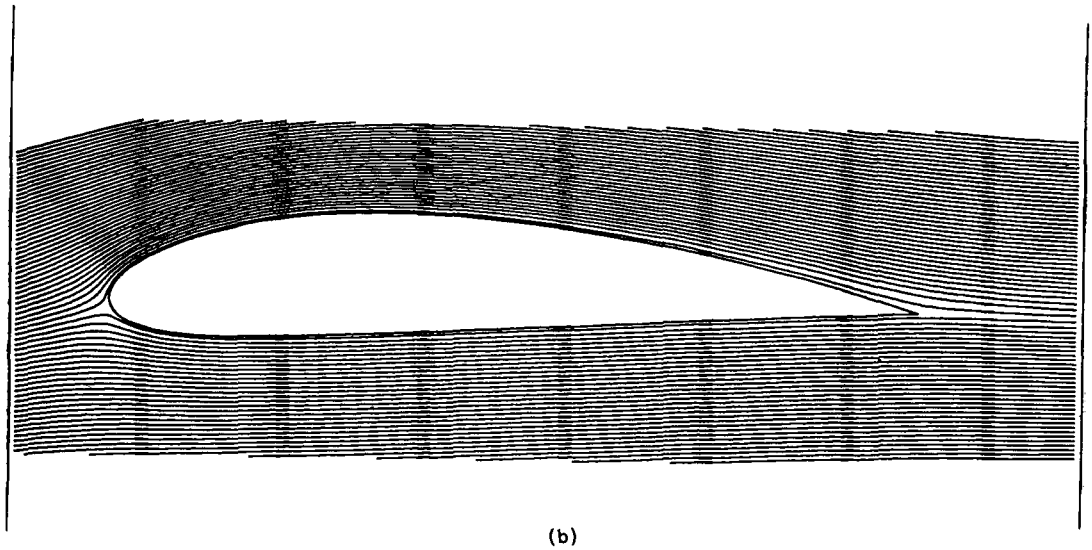

(b)

Figure 3. Streamlines of attached flow about NACA 4415: (a) $Re = 9 \times 10^6$, $\alpha = 0°$; (b) $Re = 9 \times 10^6$, $\alpha = 4°$

trailing edge. The lift coefficient increases with α even when the separated trailing edge is 30%–40% of a chord long. Eventually the separation becomes massive, the aerofoil stalls and C_L drops in a manner dependent on the aerofoil shape and Re. The maximum C_L obtained is C_{Lmax}. A sequence of computations for NACA 0012 and NACA 4415 resulted in the prediction of $C_{Lmax} = 1{\cdot}76$ for NACA 4415 at $Re = 9 \times 10^6$ and $C_{Lmax} = 1{\cdot}4$ for NACA 0012 at $Re = 6 \times 10^6$. For all calculations the transition is fixed at 4% of the chord from the leading edge. The C_p distribution and the streamlines are given in Figures 5 and 6. We see that the agreement between predicted and

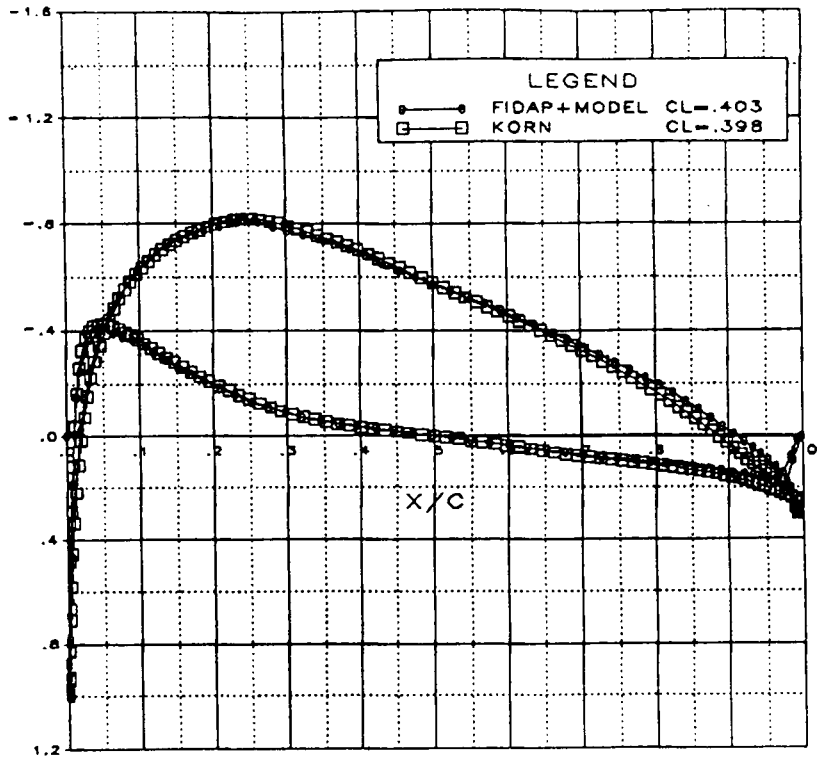

Figure 4. C_p comparison for attached flows about NACA 4415: (a) $Re = 9 \times 10^6$, $\alpha = 0°$; (b) $Re = 9 \times 10^6$, $\alpha = 4°$

(a)

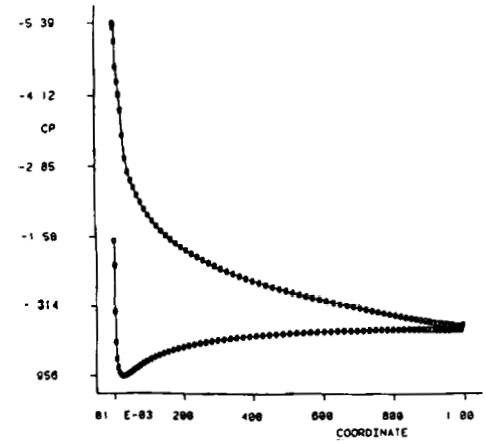

(b)

(c)

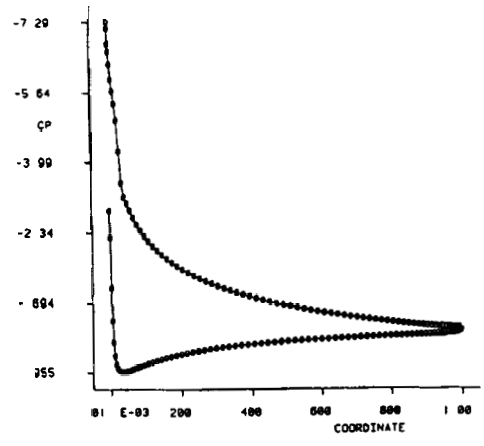

(d)

(e)

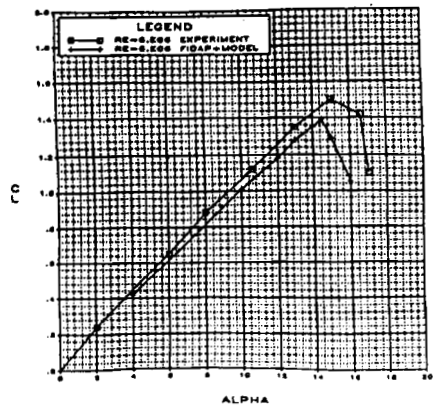

(g)

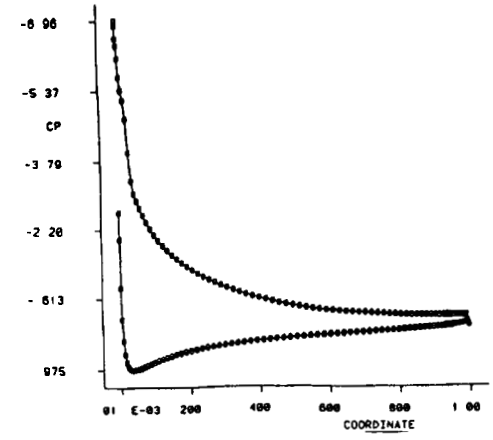

(f)

Figure 5. $C_{L\max}$ prediction for NACA 0012, $Re = 9 \times 10^6$: (a) flow streamlines for $\alpha = 12°$; (b) C_p distribution for $\alpha = 12°$; (c) flow streamlines for $\alpha = 14{\cdot}5°$; (d) C_p distribution for $\alpha = 14{\cdot}5°$; (e) flow streamlines for $\alpha = 15°$; (f) C_p distribution for $\alpha = 15°$; (g) C_L versus α curve

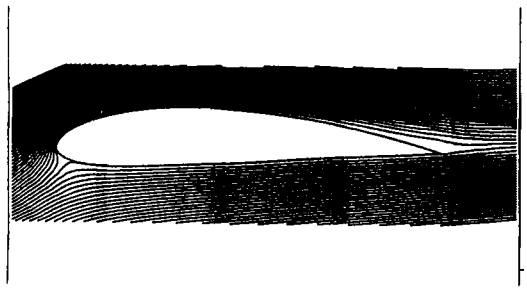

(a)

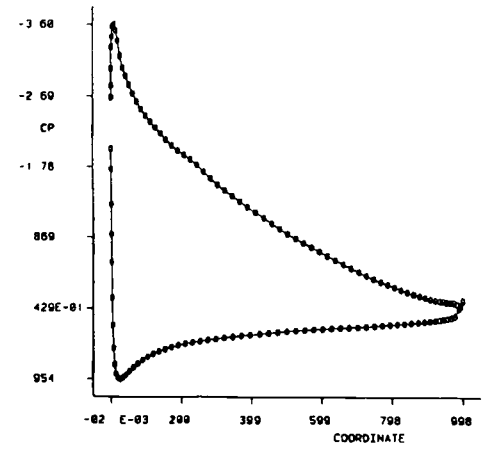

(b)

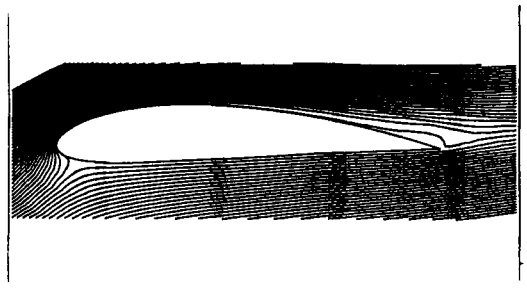

(c)

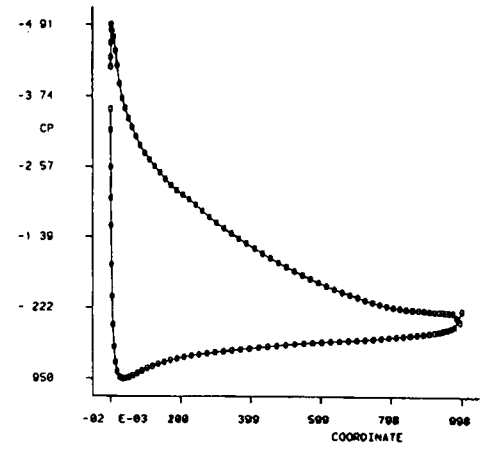

(d)

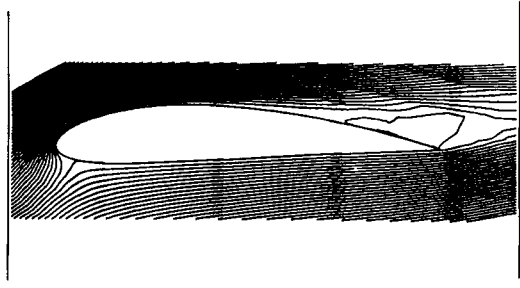

(e)

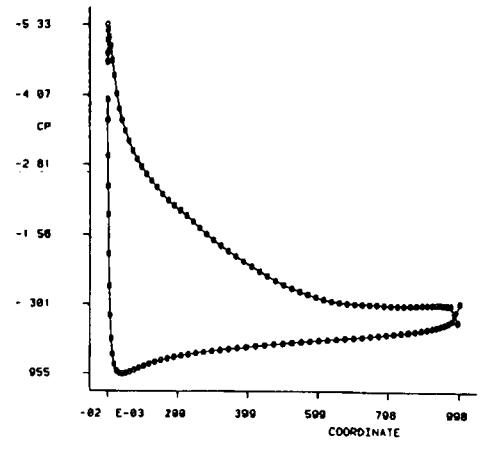

(f)

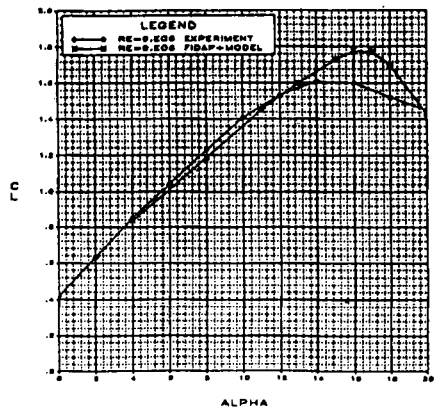

(g)

Figure 6. $C_{L\max}$ prediction for NACA 4415, $Re = 9 \times 10^6$: (a) flow streamlines for $\alpha = 13°$; (b) C_p distribution for $\alpha = 13°$; (c) flow streamlines for $\alpha = 16°$; (d) C_p distribution for $\alpha = 16°$; (e) flow streamlines for $\alpha = 18°$; (f) C_p distribution for $\alpha = 18°$; (g) C_L versus α curve

experimental C_{Lmax} is good. It is seen that before reaching C_{Lmax} the flow is attached. At C_{Lmax} there is moderate separation and beyond C_{Lmax} there is massive separation and the flow in reality is highly unsteady.[9]

The effect of Reynolds number on C_{Lmax} prediction using the Baldwin–Lomax model is shown in Figures 6 and 7. It is seen that for $Re = 3 \times 10^6$ the agreement between computed and experimental results is not as good as the comparison for $Re = 9 \times 10^6$. We note that the gradual loss of lift after stall is computed better for the case of $Re = 9 \times 10^6$ than for $Re = 3 \times 10^6$. This is to be expected since the turbulence model is suitable for higher Reynolds numbers.

Laminar separation bubble computation

Aerofoils such as NACA 4415 and NACA 0012 develop a minimum pressure peak followed by an adverse pressure gradient at the leading edge as the angle of attack increases. The laminar boundary layer immediately undergoes transition to turbulent flow. For such flow calculations the transition is fixed at 4% of the chord downstream from the minimum pressure. For other aerofoils there is laminar separation after minimum pressure for a wide range of angles of attack. The laminar flow separates, creating a short bubble, and immediately undergoes transition to turbulent flow with reattachment. The calculation of such a flow is very difficult because the start and length of the transition region are not known in advance. The calculation must correctly simulate the strong interaction between the bubble inside the boundary layer and the external

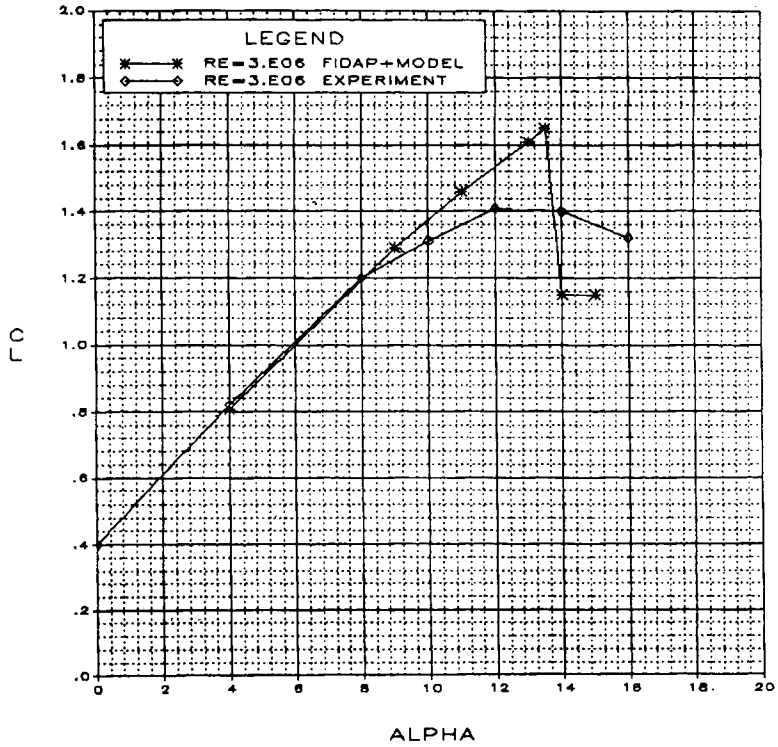

Figure 7. Reynolds number effect on C_{Lmax} prediction, $Re = 3 \times 10^6$

flow. We have developed a procedure to calculate flows with laminar separation using FIDAP plus the incorporated model to solve the full Navier–Stokes equations with no special treatment of the bubble geometry. As far as we know, all other methods predict laminar separation bubbles using a viscid/inviscid interaction calculation and not by solving the full Navier–Stokes equations as we do.

The first step of the procedure is to solve for the laminar flow at the given Re and angle of attack. From the results of this run we get the laminar separation point (LSP, Figure 8). The second step of the procedure is to locate the farthest point downstream from the LSP where transition followed by turbulent reattachment of the laminar flow is possible (we call this point A). This is done by computing the turbulent flows for assumed different positions for point A, where the straightforward application of the Baldwin–Lomax model is started. Analysis of the results of such computations after a small number of iterations indicates either transition followed by turbulent reattachment or massive separation. Point A is the farthest downstream for which transition with reattachment is possible. The distance between the LSP and point A in the cases tested is about 5% of the chord length.

In the last step we calculate the flow by application of the Baldwin–Lomax model as described above by formulae (6)–(10), starting at point A. Analysis of the results of this computation shows that the wall shear stress decreases downstream from the LSP and at point A is still an appreciable fraction of the laminar wall shear stress before the LSP. In this case the Baldwin–Lomax model is capable of suppressing laminar separation and of reattaching the flow to close the bubble and to build a turbulent boundary layer.

We have considered two types of laminar aerofoils, PR7 and P250 (Figure 9), developed and tested at IAI. For the PR7 aerofoil we apply the procedure as described above. The results are shown in Figure 10. For the P250 aerofoil the bubble prediction is more difficult.

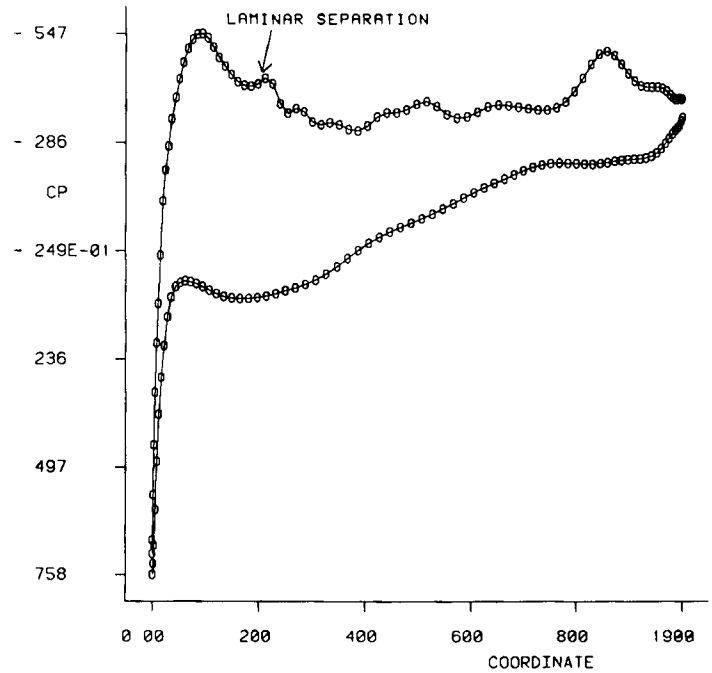

Figure 8. Laminar separation point location

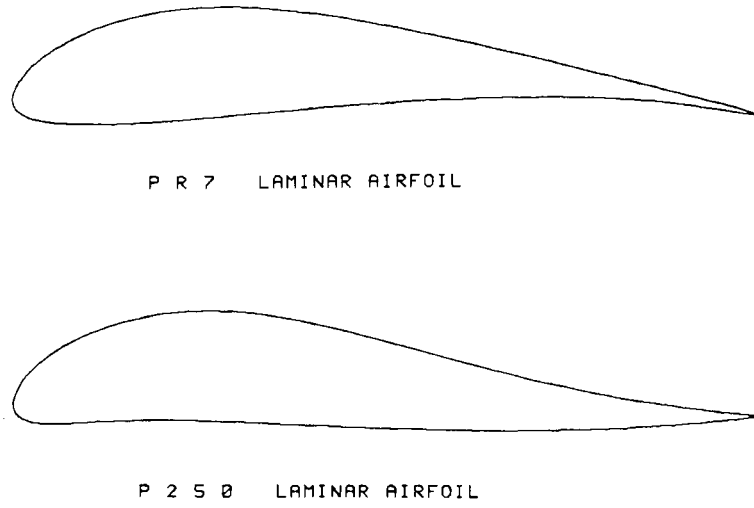

Figure 9. Different types of laminar aerofoils

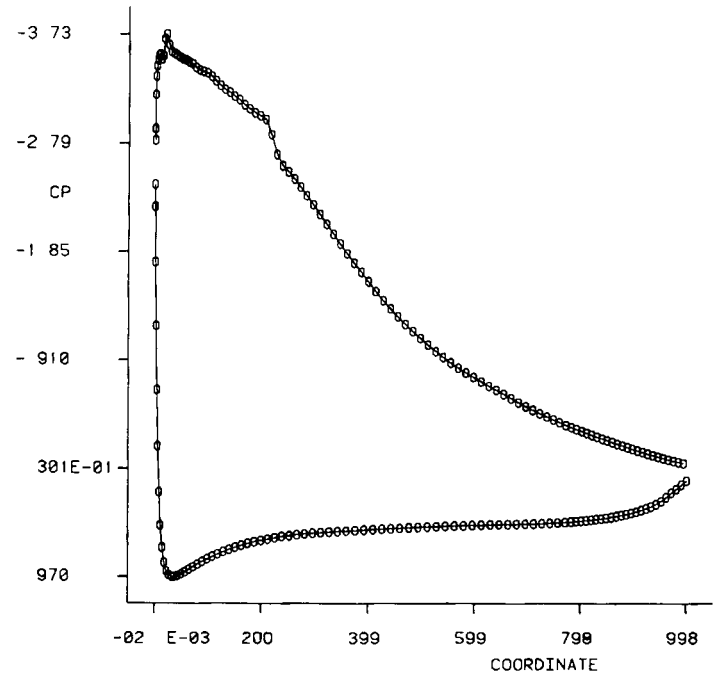

Figure 10. Laminar bubble calculation without intermittency

It turns out that for the P250 aerofoil when applying the above procedure it is necessary to prescribe the manner in which the laminar flow at the LSP undergoes transition to fully turbulent flow at point A. This is done by using the intermittency function

$$\tilde{\mu} = \mu + \gamma\, \mu_t, \tag{20}$$

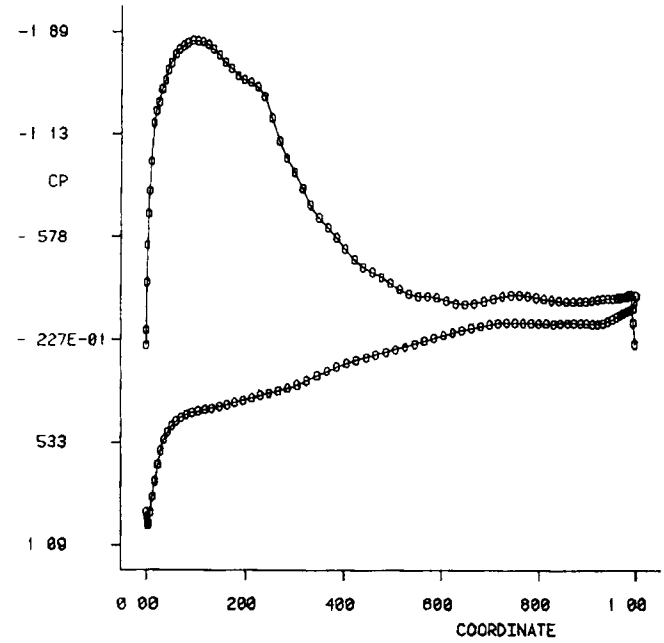

Figure 11. Laminar bubble calculation with linear intermittency

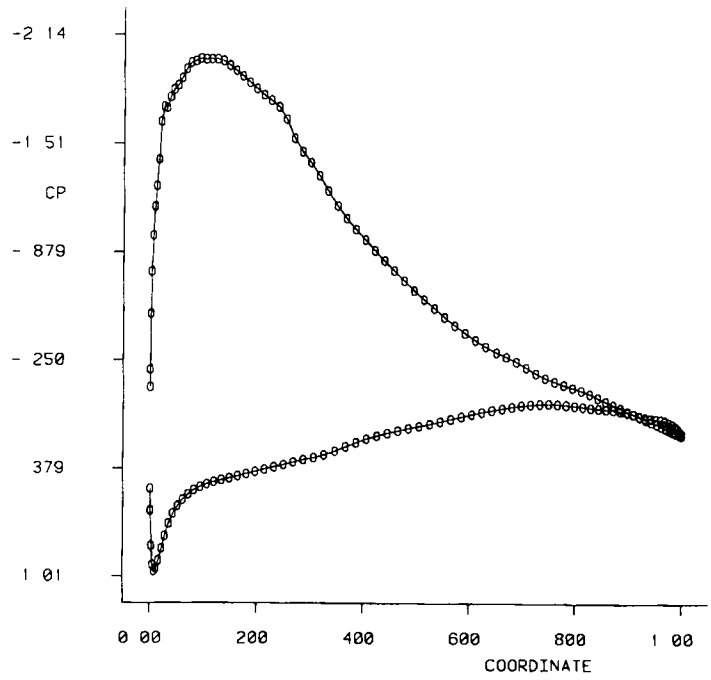

Figure 12. Laminar bubble calculation with exponential intermittency

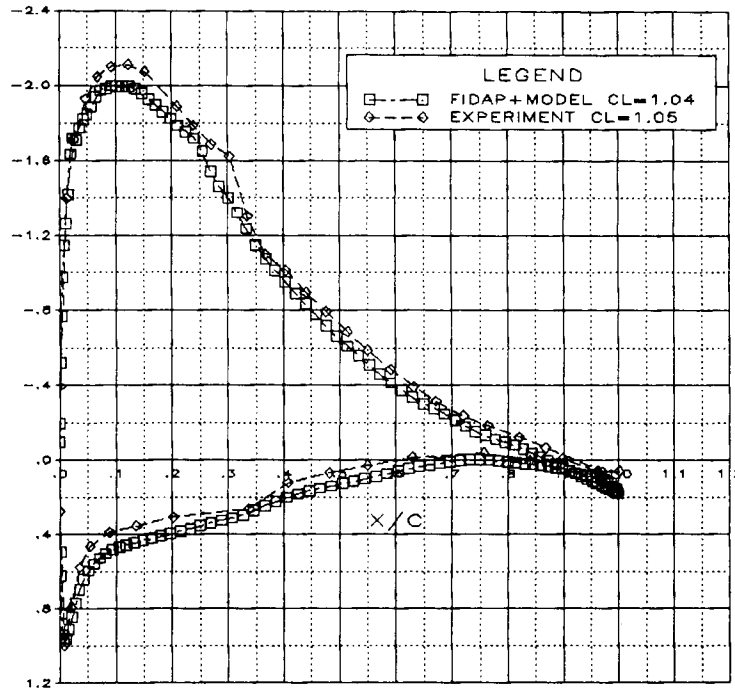

Figure 13. C_p for laminar separation bubble

where μ_t is the eddy viscosity computed by the Baldwin–Lomax model, μ is the molecular viscosity and γ is the intermittency function.

We used two types of intermittency functions, linear and exponential, to calculate the laminar separation bubble on the P250 aerofoil. The results are shown in Figures 11 and 12. It is seen that although the bubble is well predicted using the linear intermittency function, the flow is separated at the trailing edge (Figure 11). In the case of the exponential intermittency function[4, 13] the flow is not separated at the trailing edge, although the bubble is less pronounced (Figure 12). Comparison of the calculated pressure distribution using the exponential intermittency function with experimental results for an angle of attack of 6° is shown in Figure 13. The calculation is at an angle of attack of 8° because of tunnel calibration effects. It is seen that the agreement is good.

CONCLUSIONS

The eddy viscosity model incorporated at IAI into FIDAP is capable of computing attached/separated high-Reynolds-number external turbulent flows. It is possible to use FIDAP plus the model to predict laminar separation bubbles using the Navier–Stokes equations directly. In addition, we have demonstrated that using FIDAP plus the model we can predict C_{Lmax} in a reliable way for different aerofoils.

The next step using FIDAP plus the model for 2D flows is to extend the model to turbulent flows about multi-element profiles, when the added difficulty of the boundary layer/wake interaction of the various components must be considered.

APPENDIX: NOMENCLATURE

c	aerofoil chord
C_L	lift coefficient, lift/$0{\cdot}5\rho U_\infty^2$
C_{Lmax}	maximum lift coefficient
C_p	pressure coefficient, $p/0{\cdot}5\rho U_\infty^2$
F	vorticity function in turbulence model formulation
k	turbulent kinetic energy; Von Karman constant in turbulence model formulation
L	mixing length
L_∞	reference length
n	unit normal
p	pressure
R	Reynolds stress tensor
Re	Reynolds number, $\rho L_\infty U_\infty/\mu$
u_e	velocity at outer edge of boundary layer
u, v	velocities tangential and normal to surface in turbulence model formulation
u_i	Cartesian velocity components
U_∞	free velocity
x_i	Cartesian co-ordinate
x, y	co-ordinates tangential and normal to surface in turbulence model formulation
y^x	distance normal to surface where inner and outer viscosities match
α	angle of attack
β	pressure penalty parameter
γ	Klebanof intermittency function
δ	boundary layer thickness
$\delta x, \delta y$	mesh sizes tangential and normal to surface
ε	turbulent energy dissipation rate
ρ	Density
μ	molecular viscosity
$\tilde{\mu}$	total viscosity
ν	kinematic viscosity
τ	viscous stress tensor

Subscripts

i; i	tensor notation; inner layer in turbulence model formulation
k	tensor notation
o	outer layer in turbulence model formulation
∞	value at infinity
t	turbulent value

Superscripts

$(\bar{\ })$	average value
$(')$	fluctuating value

REFERENCES

1. B. E. Launder and D. B. Spalding, 'The numerical computaion of turbulent flow', *Comput. Methods Appl. Mech. Eng.*, **3**, 262–289 (1974).

2. W. Rodi, 'Examples of turbulence models for incompressible flows', *AIAA J.*, **20,** 872–879 (1982).
3. J. G. Marvin, 'Turbulence modeling for computational aerodynamics', *AIAA J.*, **21,** 941–953 (1983).
4. T. Cebeci and A. M. O. Smith, *Analysis of Turbulent Boundary Layers*, Academic Press, New York, 1974.
5. B. S. Baldwin and H. Lomax, 'Thin layer approximation and algebraic model for separated flows', *AIAA Paper 78–257*, 1978.
6. W. K. Anderson, J. L. Thomas and C. L. Rumsey, 'Application of thin layer Navier–Stokes equations near maximum lift', *AIAA Paper 84-0049*, 1984.
7. H. W. Stock and W. Hase, 'The determination of turbulent length scales in algebraic turbulence models for attached and slightly separated flows using Navier–Stokes methods', *AIAA Paper 87–1302*, 1987.
8. R. Abid, V. N. Vatsa, D. A. Johnson and B. W. Wedan, 'Prediction of separated transonic wing flows with a non-equilibrium algebraic model', *AIAA Paper 89–0558*, 1989.
9. C. L. Rumsey, 'Time dependent Navier–Stokes computations of separated flows over airfoils', *AIAA Paper 85–1684*, 1985.
10. A. N. Brooks and T. J. R. Hughes, 'Streamline upwind/Petrov–Galerkin formulation for convection dominated flows with special emphasis on the incompressible Navier–Stokes equations', *Comput. Methods Appl. Mech. Eng.*, **30,** 199–259 (1982).
11. *FIDAP Users' Manual*, Revision 4.0, Fluid Dynamics International, Inc., September 1987.
12. M. Bercovier, 'Perturbations of mixed variational problems, applications to mixed finite elements method', *RAIRO (Numer. Anal)*, **12,** 211–236 (1978).
13. V. N. Vatsa and J. E. Carter, 'Analysis of airfoil leading edge separation bubble', *NACA CR-165935*, 1982.
14. W. R. Briley and H. Macdonald, 'Numerical prediction of incompressible separation bubbles', *J. Fluid Mech.*, **69** (Part 4), 631–656 (1975).